Received: 25 February 2021 | Revised: 1 June 2021 | Accepted: 6 July 2021

DOI: 10.1049/rpg2.12254

IET Renewable Power Generation

The Institution of Engineering and Technology WILEY

ORIGINAL RESEARCH PAPER

Parametric study and optimization of a two-body wave energy converter

Xingxian Bao[1,2] | Weijie Xiao[1] | Shubo Li[1] | Gregorio Iglesias[3,4]

[1] School of Petroleum Engineering, China University of Petroleum (East China), Qingdao 266580, China

[2] National Engineering Laboratory of Offshore Geophysical and Exploration Equipment, China University of Petroleum (East China), Qingdao 266580, China

[3] MaREI, Environmental Research Institute & School of EngineeringUniversity College Cork, College Road, Cork, Ireland

[4] School of Engineering, Marine Building, University of Plymouth, Drake Circus, Plymouth PL4 8AA, UK

Correspondence
Xingxian Bao, School of Petroleum Engineering, China University of Petroleum (East China), Qingdao 266580, China.
Email: baoxingxian@upc.edu.cn

Funding information
National Natural Science Foundation of China, Grant/Award Number: 51979283; Shandong Provincial Natural Science Foundation, China, Grant/Award Number: ZR2018MEE053; Fundamental Research Funds for the Central Universities, Grant/Award Number: 20CX02313A

Abstract
The parametric study and optimization of a two-body wave energy converter (WEC) for the wave and current conditions in the region of Zhaitang Island (China) is presented. Nine parameters are considered, and their influence on the power captured by the two-body WEC is investigated following both single-parameter and multi-parameter approaches. A backpropagation neural network model is developed and applied to predict the captured power for any given values of the nine parameters and the wave frequency. Then the robust design method, also known as the Taguchi method, is implemented to study the comprehensive effects of the parameters on the power output of the device. Moreover, scale model experiments are conducted to verify and confirm the influence of the principal parameters on the power output. Combining numerical simulations, a neural network model and experimental work, this study provides an optimization programme for the main parameters of the device in the target sea region and, at a more general level, references for two-body WEC designs based on specific sea states.

1 | INTRODUCTION

The international community has paid more and more attention to issues such as ensuring energy security, protecting the ecological environment, and responding to climate change. China just announced its intention to strive to reach the peak of carbon dioxide emissions before 2030, and strive to achieve carbon neutrality before 2060 [1]. Accelerating the development and utilization of ocean energy, especially wave and tidal energy, has become a universal consensus and concerted action of coastal countries and regions around the world [2]. Wave energy has the largest potential in Europe and worldwide, and in-depth study of the characteristics of the wave energy converter (WEC) will make a significant contribution to improving the efficiency of resource collection and conversion [3].

Wave energy can be captured in a number of ways through the use of different converters, such as point absorbers, attenuators, overtopping, oscillating wave surge convertors, and oscillating water columns [2, 3]. Many different types of WECs have been designed, but only a small proportion of these have reached the full-scale prototype stage so far [2]. Among the various forms of WECs, point absorber WECs have attracted extensive attention because of their simple structure and high conversion efficiency [4], which consist of single-body and two-body point absorber types.

Intensive research has been devoted to improving the wave energy conversion efficiency of the single-body point absorber WECs. The hydrodynamic characteristics of the float with different shapes such as square, cylindrical and rectangular float have been studied widely [5, 6], including the wave radiation

[7–9], the wave diffraction [9, 10] and the viscous and friction effects [11, 12]. In addition to the geometry of the float [13], optimization analyses for single-body point absorber WECs have been carried out on the layout of the mooring lines [14, 15], the mass distribution of the float [16], the draft and diameter [17] and the PTO damping [17, 18], etc.

The single-body point absorber WECs usually require a larger mass and scale to reduce their natural frequency so as to match the wave frequency as far as possible and thus maximize the absorption power, but this increased mass has a negative impact on the cost of energy. To solve this problem, some control methods [19, 20] were also developed to maximize harvested power for point absorber WECs.

Another way to develop a resonant WEC is to add a submerged body under the floating buoy to create a two-body point absorber WEC, where the energy is extracted through the relative motion of the two bodies [21–23]. Some research has been carried out regarding the optimization of the two-body point absorber WECs. Candido and Justino [24] analysed the operating characteristics of a coaxial two-body WEC that only performs heave motion under linear damping load conditions. The numerical results showed that the wave frequency and the restraining measures on the motion amplitude are the main factors affecting its conversion efficiency. Shami et al. [25] used the Taguchi method to analyse the influence of seven parameters on the captured power of a two-body WEC only considering heave motion. Liang and Zuo [21] studied the linear viscous damping and hydrodynamic simplification of the two-body WEC in the frequency domain and proposed an optimized design to obtain the maximum output power. Muliawan et al. [26] investigated a two-body WEC with relaxed mooring in the regular and random wave conditions and found that the mooring force has little effect on the wave energy absorbed by the buoy, as long as the length of the mooring lines can accommodate the heave motions of the device. Martin et al. [27] presented numerical and experimental analysis on the optimum design of a two-body WEC. The results showed the two-body WEC could produce twice as much energy as the single-body WEC with the same float.

The relevant parameters of a WEC are, generally speaking, not independent of one another. For instance, the size and geometry of the buoys can influence the hydrodynamic performance of the WEC, which in turn can affect the optimization of PTO coefficients. Hence, optimizing a WEC requires a comprehensive analysis of a wide range of parameters related to the design of the device and the environmental conditions of the sea area where the WEC will be deployed.

Although some work that has been conducted on the optimization of two-body point absorber WECs based on a certain parameter or a few parameters, a comprehensive optimization including several parameters that affect the output power over a large enough wave frequency bandwidth has not been carried out so far. This is the motivation for the parametric study and optimization presented in this work, with a focus on the effects of nine parameters on the captured power of a two-body point absorber WEC, including: the buoy's size, the distance between two floats, the PTO damping, the PTO stiffness, the current velocity, the wave height, the angle between the anchor chain and the plumb line, the angle between the incident wave direction and the projection of the anchor chain on the horizontal plane, and the angle between the incident wave direction and the current.

The target sea conditions off Zhaitang Island, China, the basic two-body WEC model and the parametric study methods, including the backpropagation (BP) neural network, and the robust design method are briefly introduced in Section 2. The parametric studies considering the influences of individual parameters and groups of parameters on the captured power of the device are presented in Section 3. Section 4 illustrates the scale model experimental results in a wave-current tank. Based on the numerical and experimental parametric studies of the two-body point absorber WEC, the optimal combination of parameters for deployment off Zhaitang Island (China) is determined in Section 5. Finally, conclusions are drawn in Section 6.

2 | MODEL AND METHOD

2.1 | Target sea region and basic WEC model

The target sea region of our study is located off Zhaitang Island, Qingdao, Shandong province, China, which is in the north of the Yellow Sea, facing the open sea in the east and south. This ocean energy test base, the largest in northern China since 2012, focuses on the development of multi-energy complementary and intelligent independent energy systems, including wave energy, tidal energy and current energy devices, low-cost ocean energy transmission and transformation equipment, and other marine renewable energy technology. The water depth suitable for wave energy generation off Zhaitang Island is about 30 m. The mean significant wave height is 0.6 m, mean wave period is 3.3 s, and mean current velocity is 0.9 m/s.

The basic two-body WEC model presented in this paper is illustrated in Figure 1, consisting of a cylindrical floater and a spherical submerged body with the same radius. The PTO system is placed between the two buoys and makes use of the relative movement of the two buoys to generate electricity. The converter is fixed onto the seafloor by four tensioned anchor chains. This study focuses on investigating the influence of nine parameters on the captured power by the WEC, such as the buoy's radius R, the distance between two buoys D, the PTO damping C, the PTO stiffness K, the current velocity V, the wave height H, the angle between the anchor chain and the plumb line α, the angle between the incident wave direction and the projection of the anchor chain on the horizontal plane β, the angle between incident wave direction and the current γ.

2.2 | Dynamics analysis

Since the software Ansys Aqwa [28] is used to conduct the numerical simulation in this study, the equations of motion for the two-body WEC and the computation methods applied in Ansys Aqwa are briefly introduced here. Newton's second law

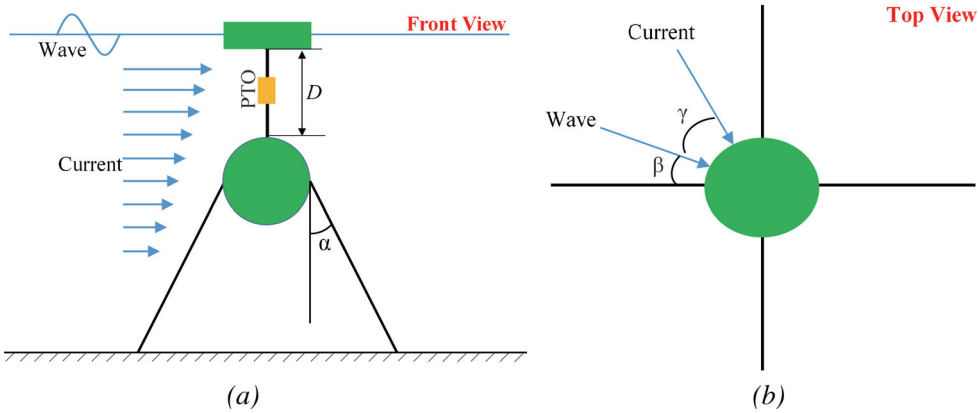

FIGURE 1 Sketch of the two-body WEC. (a) Front view, (b) top view

is used in the two-body WEC system considering solely two degrees of freedom (Figure 1), where X_j, X_j' and X_j'' denote the displacement, velocity and acceleration, respectively, $j = 1$ denotes the floater, and $j = 2$ denotes the submerged buoy.

For the floater:

$$m_1 X_1''(t) = F_{r1}(t) + F_{pto}(t) + F_s(t) + F_i(t) + F_{e1}(t) + F_{c1}(t) \tag{1}$$

For the submerged body:

$$m_2 X_2''(t) = F_{r2}(t) - F_{pto}(t) - F_i(t) + F_{e2}(t) + F_{c2}(t) + F_m(t) \tag{2}$$

where m_j represents the physical dry mass; F_{rj} represents the radiation force, according to Cummins' equation [29, 30], the radiation force is a differential equation of order two with a convolution integral, $F_{rj}(t) = -m_{aj}X_j''(t) - \int_0^t K_j(t-\tau)X_j'(\tau)d\tau$, where m_{aj} represents the added mass, $\int_0^t K_j(t-\tau)X_j'(\tau)d\tau$ is the convolution integral, and K_j is the retardation function. Based on the radiation damping coefficients $r_j(\omega)$for every possible frequency, K_j can be expressed as$K_j(t) = \frac{2}{\pi}\int_0^\infty r_j(\omega)\cos(\omega t)d\omega$. $r_j(\omega)$ can be provided through frequency analysis in Ansys Aqwa for a set of predefined frequencies$\{\omega_n\}$; F_{pto} represents the PTO force; F_s represents the static restoring force$F_s(t) = -\rho g A_w X_1(t)$, where $\rho$is the water density, g is the gravity acceleration, and A_w represents the waterline surface area. For the submerged body, F_s is 0, given the balance between gravity and buoyancy; F_i represents the force caused by the hydrodynamic interactions between the two buoys, which can be neglected when the submerged body is deployed far enough from the floater;F_{ej} represents the wave load on the two buoys; F_{cj}represents the current load, which can be obtained as the drag force$F_{cj}=\frac{1}{2}C_D\rho A v_j^2$, where$C_D$is the drag coefficient, $A$is the cross-sectional area of the buoy perpendicular to the direction of current motion and$v_j$is the relative velocity between the current and the buoys; and F_m represents the mooring forces exerted on the submerged body, which can be calculated in Ansys Aqwa by setting the cable mooring type and its properties, including the section properties and the section hydrodynamic properties. The PTO force F_{pto} can be expressed as

$$F_{pto} = -F_d - F_k \tag{3}$$

and F_d F_k are linear forces:

$$F_d = c_p\left(X'_1 - X'_2\right) \tag{4}$$

$$F_k = k_p(X_1 - X_2) \tag{5}$$

where k_p and c_p represent the PTO's stiffness and damping coefficients, respectively.

Equations (1) and (2) can be rewritten, respectively, as

$$\begin{aligned}&(m_1 + m_{a1})X''_1(t) + \int_0^t K_1(t-\tau)X'_1(\tau)\,d\tau \\ &+ c_p\left(X'_1(t) - X'_2(t)\right) + \left(\rho g A_w + k_p\right)X_1(t) - k_p X_2(t) \\ &- F_i(t) = F_{e1}(t) + F_{c1}(t)\end{aligned} \tag{6}$$

and

$$\begin{aligned}&(m_2 + m_{a2})X''_2(t) + \int_0^t K_2(t-\tau)X'_2(\tau)\,d\tau \\ &+ c_p\left(X'_2(t) - X'_1(t)\right) + k_p(X_2(t) - X_1(t)) \\ &+ F_i(t) = F_{e2}(t) + F_{c2}(t) + F_m(t)\end{aligned} \tag{7}$$

K_j,$X_1(t)$ and $X_2(t)$ in Equations (6) and (7) can be solved based on the hydrodynamic analysis in the frequency and time domains using Ansys Aqwa for the basic WEC model. The average captured power over a period of time T can then be obtained as

$$\begin{aligned}P_{average} &= \frac{1}{T}\int_0^T F_c\left(X'_1(t) - X'_2(t)\right)dt \\ &= \frac{1}{T}\int_0^T c_p\left(X'_1(t) - X'_2(t)\right)^2 dt\end{aligned} \tag{8}$$

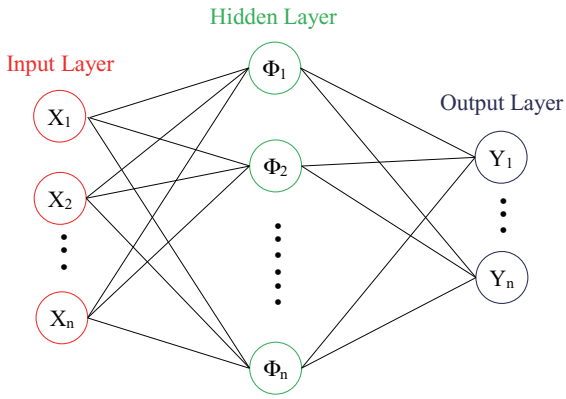

FIGURE 2 The general structure of BP neural network

2.3 | Brief introduction of BP neural network

The motion response of the two-body WEC with a combination of several parameters can be analysed by the numerical simulation software, and then the captured energy can be obtained based on Equation (8). However, in order to study the effect of each parameter of the WEC on the captured power, the computational cost would be prohibitive. In order to keep the computation time within manageable limits, the artificial neural network is trained to predict the captured power with the variation of parameters based on the simulation cases.

For the relatively small amount of data, the traditional BP neural network has strong non-linear mapping ability and enough prediction accuracy, which is applied for training and prediction in this study. The general structure of the BP neural network is described in Figure 2, which mainly consists of input layer, hidden layer and output layer, as well as signal forward propagation and error back propagation. In forward propagation, the input signal acts on the output node through the hidden layer, and the output signal is generated through non-linear transformation [31]. For example, it can be represented by the input-output relationship of the j neuron in the k layer,

$$y_j^k = f_f^k\left\{\sum_{i=1}^{n_{k-1}} W_{ij}^{(k-1)} y_i^{(k-1)} - \theta_j^k\right\},$$
$$j = 1, 2, \ldots, n_k;\ k = 2, 3, \ldots, M \tag{9}$$

where $W_{ij}^{(k-1)}$ represents the connection weight factor from the i neuron of the $k-1$ layer to the j neuron of the k layer, θ_j^k represents the threshold of the neuron, f_f^k represents the function of BP network node, n_k represents the number of neurons in the k layer, and M represents the total number of layers of the neural network model, $M \geq 2$.

If the actual output does not agree with the expected output, the process of back-propagation of errors will be initiated. The process of error back-propagation from output to input modifies the corresponding network parameters by means of the gradient descent method. The ultimate goal is to determine the suitable W and θ for the minimum total error of the network through iterations,

$$\begin{cases} W(k+1) = W(k) - \eta\dfrac{\partial E}{\partial W(k)} \\ \theta(k+1) = \theta(k) - \eta\dfrac{\partial E}{\partial \theta(k)} \end{cases} \tag{10}$$

where η refers to the network learning factor, and E is the error function in the process of neural network training.

2.4 | The robust design method

The robust design method is a three-stage design method created by Genichi Taguchi in 1950′s, also called Taguchi method. This method is an effective multi-parameter analysis method and has been widely used for process optimization in the industry [25, 32]. The robust design method can assess the performance of a system with different parameters, as well as the influence level of each parameter. The robust design method is applied in this work to study the comprehensive influence of nine parameters on the power captured by the two-body WEC.

3 | PARAMETRIC STUDY

3.1 | The influence of individual parameter on captured power

In this section, the independent influence of the nine parameters such as $R, D, C, K, V, H, \alpha, \beta$ and γ on the power captured by the two-body WEC will be investigated. Table 1 presents the nine systems, each with one variable and eight invariable parameters, simulated using Ansys Aqwa software. For example, in the first system, the effect of parameter R on captured power is studied. Hence, R is variable, and the other parameters are fixed as follows: D is 3 m, C is 3000 N·s/m, K is 300 N/m, V is 0.9 m/s, H is 0.6 m, α is 40°, β is 0°, γ is 0°. In each system, the variable parameter used in this simulation study is listed in Table 2. In this study the ratio of the draft to the radius of the floater in each system is constant, 0.65. In addition, the wave frequency in the range of [0.1, 0.5] Hz is also considered for the simulation of each system, but the intervals of the wave frequency are not same for all the systems.

Because the distance between the submerged body and the floater is small (no more than 5 m), the hydrodynamic interactions between the two buoys are considered with the Ansys Aqwa software by analysing the influence of one buoy's flow field on the other's [28]. First, the hydrodynamic coefficients, such as added mass and radiation damping, are obtained in the frequency domain analysis by taking into account the unit wave amplitude. Then, the equations of motion in the time domain, Equations (6) and (7), are solved considering the total force on the buoys, including the wave, current and mooring force.

In all, 450 simulation cases related to 9 systems were conducted. As an example, Figure 3 shows the relative displacement time history of two floats corresponding to the system 6

TABLE 1 Parameter values corresponding to the nine systems

System	R (m)	D (m)	C (N·s/m)	K (N/m)	V (m/s)	H (m)	α (°)	β (°)	γ (°)
1	Variable	3	15,000	3600	0.9	0.6	50	0	0
2	2	Variable	15,000	3600	0.9	0.6	50	0	0
3	2	3	Variable	3600	0.9	0.6	50	0	0
4	2	3	15,000	Variable	0.9	0.6	50	0	0
5	2	3	15,000	3600	Variable	0.6	50	0	0
6	2	3	15,000	3600	0.9	Variable	50	0	0
7	2	3	15,000	3600	0.9	0.6	Variable	0	0
8	2	3	15,000	3600	0.9	0.6	50	Variable	0
9	2	3	15,000	3600	0.9	0.6	50	0	Variable

TABLE 2 Variable parameter values corresponding to the nine systems

Variable	1	2	3	4	5	6	7	8	9	10
R(m)	1	1.5	2	2.5	3					
D(m)	1	2	3	4	5					
C(N·s/m)	1000	3000	6000	9000	12,000	15,000	18,000	21,000	24,000	27,000
K(N/m)	300	1200	2400	3600	4800					
V(m/s)	0.1	0.5	0.9	1.3	1.7	2.1				
H(m)	0.2	0.4	0.6	0.8	1	1.2				
α(°)	10	20	30	40	50	60	70			
β(°)	0	10	20	30	40					
γ(°)	0	30	60	90	120	150	180			

with variable parameter wave height 1.0 m and wave frequency 0.1 Hz. The relative velocity of two floats can be obtained by derivation of the relative displacement and finally the captured power corresponding to system 6 with the specific parameters can be calculated using Equation (8).

In order to predict the captured power more accurately with the variation of nine parameters as well as wave frequencies, the BP neural network is constructed based on the 450 simulation cases. The number of input layer, hidden layer and output layer units is set to 10, 8 and 1, respectively. The 450 cases are divided into a training dataset (70% of the cases) and a test or validation dataset (30% of the cases). After about 300 iterations, the BP neural network has converged.

Excellent agreement may be observed between the predicted and simulated data of the training dataset, test dataset and total dataset in Figure 4(a–c), respectively. The correlation coefficient (R) is, in the three cases, close to unity. Figure 5 illustrates the prediction errors of all the 450 cases. In 93.3% of the cases, the error is below 10%. In only 1.3% of the cases is the error greater than 20%, and these are cases with relatively small cap-

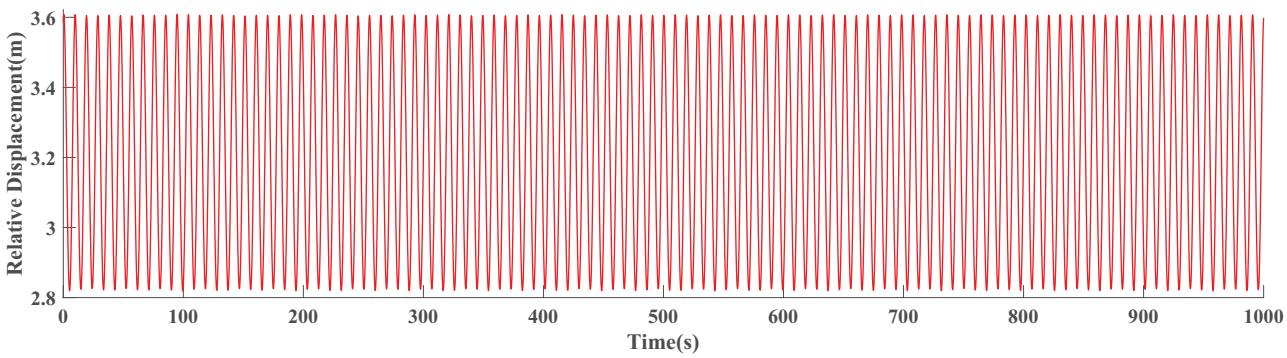

FIGURE 3 Relative displacement of two floats over time

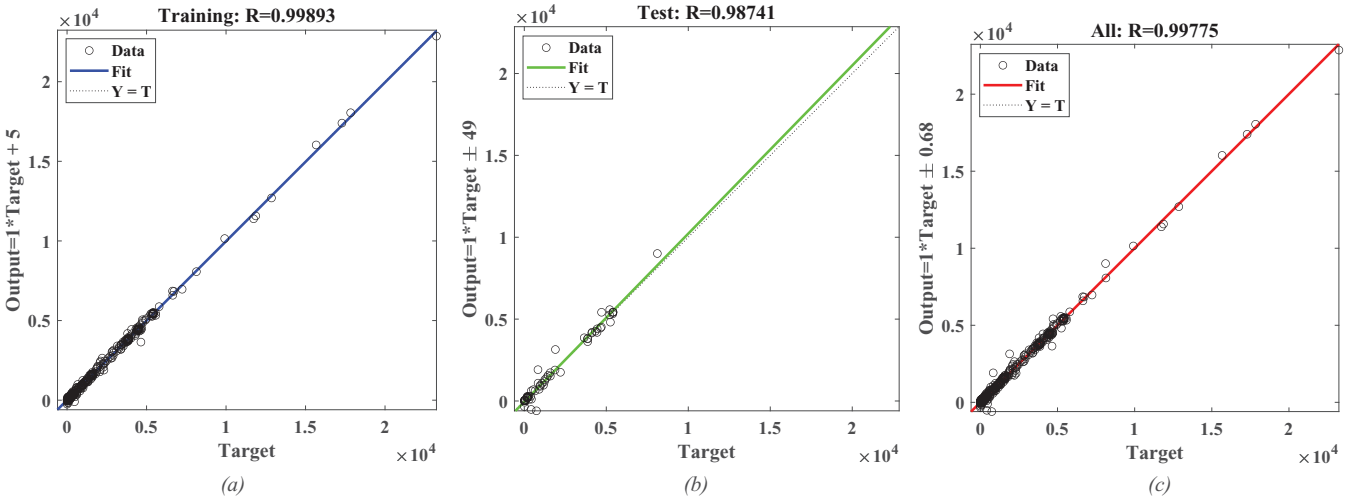

FIGURE 4 Goodness of fit and correlation coefficient (R) of BP neural network with the (a) training, (b) test and (c) total dataset

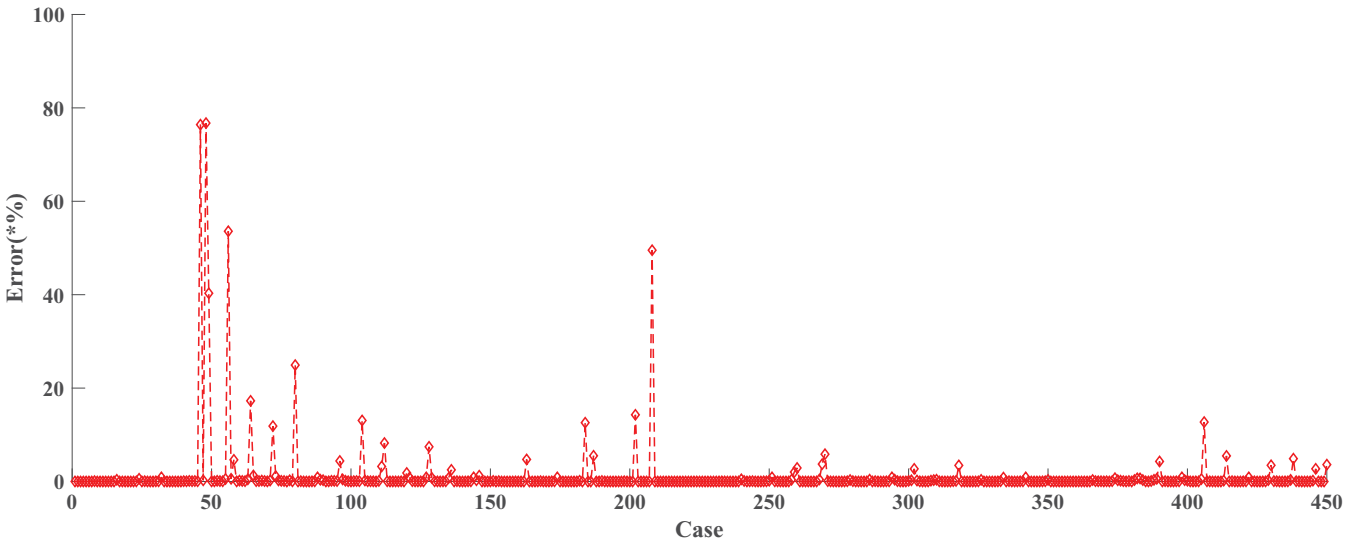

FIGURE 5 Prediction errors of 450 cases

tured power. In fact, the cases of interest for real-life applications are those with relatively high captured power, and the prediction errors for these cases are very small.

Furthermore, in order to study the influence of individual parameters on the power captured by the WEC more accurately, the trained BP neural network is applied to predict the captured power with 100 different values of the variables, between the maximum and minimum values in Table 2, as well as 10 wave frequencies in the range of (0, 0.5] Hz for each of the 9 systems, i.e. about 9000 cases are considered in the prediction. Figure 6 shows the variation in predicted output power with respect to the nine individual parameters and the wave frequency.

From Figure 6(a) it can be seen that, in the range of [1, 3] m, the larger the radius of the buoy, the more wave energy it captures, which agrees with the conclusion in Ref. [4] for the constant draft to radius ratio. In addition, it is found that the range of wave frequencies considered is 0.2–0.3 Hz. Since the simulated height of the cylinder increases with the radius to maintain the water plane in the middle of the cylinder, and to ensure the draft to radius ratio is kept at 0.65 in this study, the natural frequency of the WEC will decrease as the radius increases, and therefore the wave frequency at which maximum output power is obtained will also decrease. The mean wave frequency in Zhaitang Island is 0.3 Hz, and therefore the radius of the buoy should not exceed 3 m.

Figure 6(b) shows the output power related to the distance D between two buoys. It can be found that with the increase of the distance$D$, the wave frequency corresponding to the maximum output power does not change significantly but remains around 0.275 Hz, while the maximum captured power will first increase and then remain stable. When the distance is about 3 m, the output power begins to reach the maximum value 5400 W.

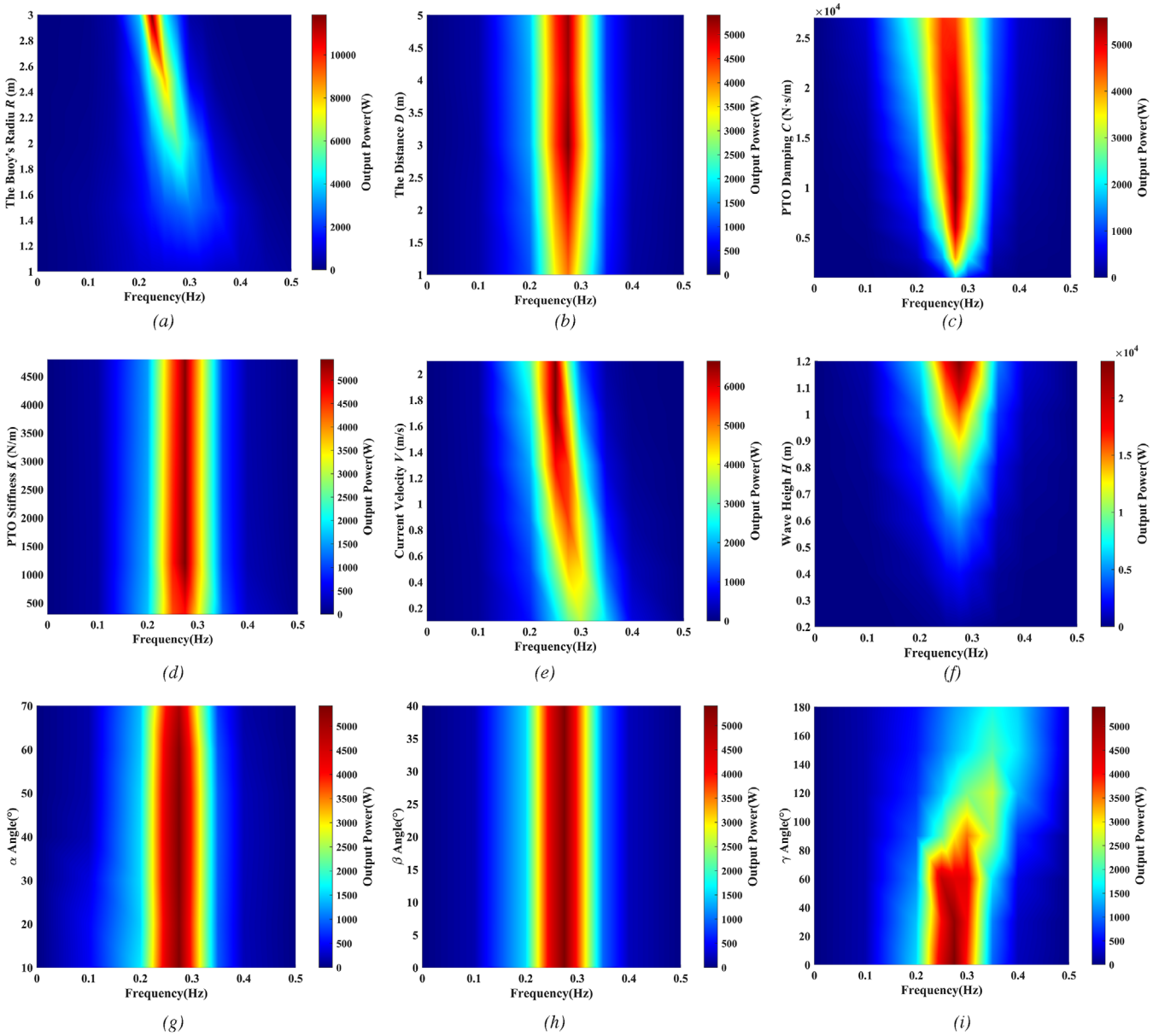

FIGURE 6 Output power related to 9 individual parameters and wave frequencies

It is known that the increase of the device's PTO damping will hinder the relative movement of the two buoys and reduce their relative velocity. On the other hand, according to Equation (8), the PTO damping is positively related to the captured power of the device. This means that there will be an optimum range of PTO damping that will maximize power output. As shown in Figure 6(c), the output power of the device increases rapidly as the PTO damping increases around the wave frequency 0.275 Hz, and then reaches the maximum value of 5400 W and remains stable in the PTO damping range of 9000–15,000 N·s/m. When the PTO damping continues to increase, the maximum output power begins to decrease.

Figure 6(d) shows the output power related to the PTO stiffness K. When the PTO stiffness is 300–1200 N/m, the maximum captured power of the device is relatively low, about 4700 W. When the PTO stiffness is between 1200 and 4800 N/m, the maximum captured power remains stable at 5400 W. This is because, although the change of PTO stiffness will affect the relative movement speed of the two buoys, when the PTO stiffness is much less than the static restoring stiffness $\rho g A_w$ (see Equation (6)), the relative movement speed of the two floats will not be greatly affected. In other words, the change of PTO stiffness within that range has no significant effect on the captured power of the device.

The influence of the current velocity V on the output power is illustrated in Figure 6(e). Besides the waves, the current is also a main factor that causes the float to oscillate. Assuming that the direction of the incident waves and current is the same in

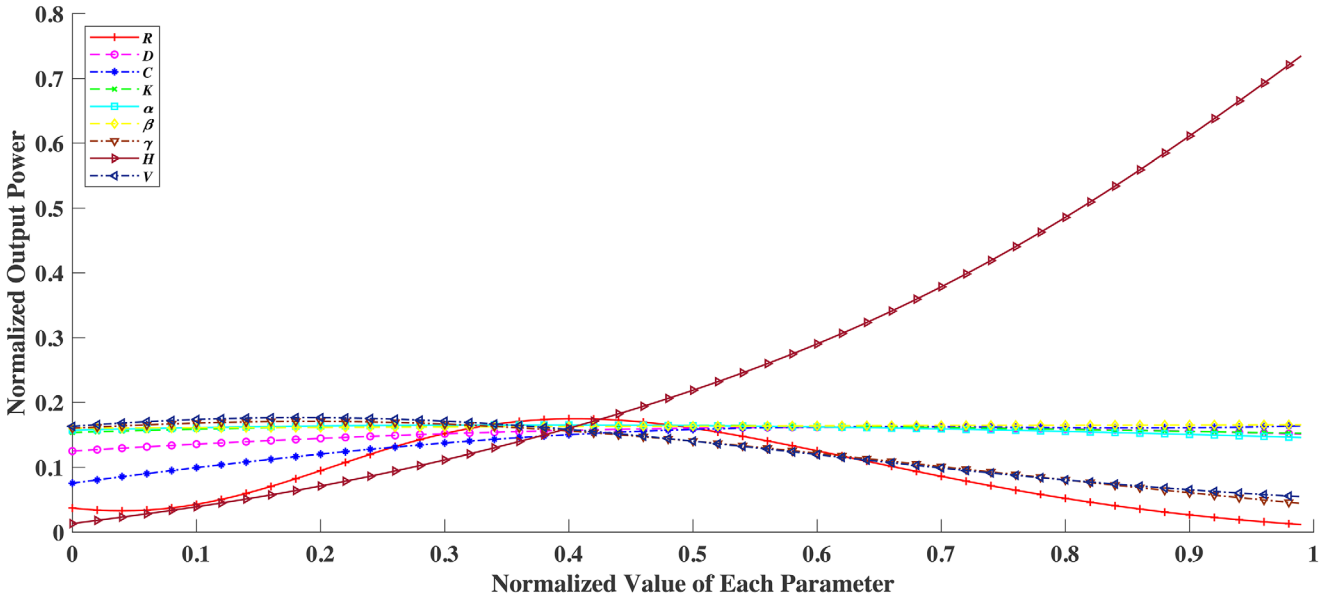

FIGURE 7 Predicted influence of each parameter on the captured power using BP neural network

this system, it can be seen that the wave frequency related to the maximum captured power changes with the current velocity. The greater the current velocity, the smaller the wave frequency corresponding to the maximum captured power of the device. In addition, when the current velocity is small, with the increase of current velocity, the captured power of the device increases rapidly. But once the current velocity has reached a certain level (≈1.7 m/s), the captured power reaches the maximum value of 6600 W, and then remains stable as the current velocity increases.

As shown in Figure 6(f), the captured power of the device increases greatly as the wave height increases. When the wave height is 0.2 m, the captured power of this system is only 500 W, and when the wave height reaches 1.2 m, the captured power increases to 23,000 W, which fully highlights the influence of the wave height on the captured power of the device.

Figure 6(g) presents the effect of the angle between the anchor chain and the plumb line α on the output power. Considering the actual conditions, this angle will not be too large, so the maximum angle is set to 70° in the numerical simulation and neural network prediction. It is found that when the angle between the anchor chain and the plumb line is in the range of 10–65°, the maximum captured power remains stable at about 5400 W. Given that the main function of the anchor chain connected with the submerged body is to limit the movement of the buoy to a certain area, and the fact that the anchor chain is relatively long and has a certain tensile capacity, the angle α will not have a great impact on the relative motion of the two buoys, and therefore will not affect the captured power significantly, in agreement with the findings of Muliawan et al. [26]. As long as the length of the mooring lines can accommodate the motions of the device due to first-order wave forces, especially in heave for the Wavebob-type WEC, the effect of the mooring would be insignificant [26].

The influence of the angle between the projection of the anchor chain on the horizontal plane and the incident wave direction β on the output power is shown in Figure 6(h). Because four anchor chains are used in this study, the angle β varies from 0° to 45°. It can be seen that with the change of the angle, the captured power is stable at 5400 W, similar to Figure 6(g). This indicates that the layout of the anchor chains has little impact on the captured power of the WEC.

Figure 6(i) shows the relations of the output power and the angle between the incident wave direction and the current γ. It can be found that when the angle γ is between 0° and 50°, the captured power is relatively large, and the maximum value is about 5400 W. However, the captured power decreases rapidly when γ is 80–180°. On the whole, a small angle between the wave and current or, even better, coincident wave and current directions, is beneficial to the output power.

Considering that the mean wave frequency of the target sea region is 0.3 Hz, the BP neural network is also applied to predict the influence of each parameter on the captured power based on the wave frequency 0.3 Hz. Note that each parameter and the captured power are all normalized to [0, 1]. Figure 7 shows the comparison of the influence level of each parameter on the captured power. It is found that the wave height H has the largest impact followed by the buoy's radius R, current velocity V, the angle between the direction of wave and current γ, and the PTO damping C. The other four parameters, such as the distance between two floats D, the PTO stiffness K, the angle between the anchor chain and the plumb line α, and the angle between the projection including the anchor chain in the horizontal plane and the direction of the wave β have little effect on the captured power. Additionally, it is seen that the wave height is positively correlated to the captured power, while the captured power increases first and then reduces with the increase in the buoy's radius.

TABLE 3 Robust design method using the L32 matrix

System	R	D	C	K	H	V	α	β	γ
1	1	1	1	1	1	1	1	1	1
2	1	2	2	2	2	2	2	2	2
3	1	3	3	3	3	3	3	3	3
4	1	4	4	4	4	4	4	4	4
5	2	1	1	2	4	4	2	3	3
6	2	2	2	1	3	3	1	4	4
7	2	3	3	4	2	2	4	1	1
8	2	4	4	3	1	1	3	2	2
9	3	1	2	3	3	4	4	2	1
10	3	2	1	4	4	3	3	1	2
11	3	3	4	1	1	2	2	4	3
12	3	4	3	2	2	1	1	3	4
13	4	1	2	4	2	1	3	4	3
14	4	2	1	3	1	2	4	3	4
15	4	3	4	2	4	3	1	2	1
16	4	4	3	1	3	4	2	1	2
17	1	1	4	1	2	3	4	3	2
18	1	2	3	2	1	4	3	4	1
19	1	3	2	3	4	1	2	1	4
20	1	4	1	4	3	2	1	2	3
21	2	1	4	2	3	2	3	1	4
22	2	2	3	1	4	1	4	2	3
23	2	3	2	4	1	4	1	3	2
24	2	4	1	3	2	3	2	4	1
25	3	1	3	3	4	2	1	4	2
26	3	2	4	4	3	1	2	3	1
27	3	3	1	1	2	4	3	2	4
28	3	4	2	2	1	3	4	1	3
29	4	1	3	4	1	3	2	2	4
30	4	2	4	3	2	4	1	1	3
31	4	3	1	2	3	1	4	4	2
32	4	4	2	1	4	2	3	3	1

3.2 | The influence of multi-parameter on captured power

In fact, the influence of these parameters on captured power is not independent, so it is necessary to analyse the comprehensive influence of multi-parameter on captured power. In what follows, the robust design method is applied and four levels of each parameter is selected to construct a L32 matrix (see Table 3), in which each system consists of nine parameters with different levels. Table 4 shows the specific values of each parameter corresponding to four levels, respectively.

Based on the 32 numerical simulation cases with the related parameters in Table 3, the captured power can be obtained respectively. The average of the maximum captured power corresponding to each parameter with each level is listed in Table 5 (columns 2–5) and the range of the which is listed in column 6, then the effect value listed in column 7 is calculated using the maximum captured power value in the four levels divided by the range, which represents the influence level of a certain parameter on the captured power.

TABLE 4 The specific values of each parameter at 4 levels

Parameter	Level 1	Level 2	Level 3	Level 4
R(m)	1.5	2	2.5	3
D(m)	1	2	3	4
C(N·s/m)	3000	9000	15,000	21,000
K(N/m)	500	1500	2500	3500
V(m/s)	0.2	0.8	1.4	2
H(m)	0.2	0.6	0.8	1.2
α(°)	10	30	50	70
β(°)	0	15	30	45
γ(°)	0	45	90	180

From Table 5 it can be seen that the four parameters such as the wave height H, the PTO damping C, the buoy's radius R, and the current velocity V, have the significant impacts on the captured power, with the effect value being 97.4%, 73.3%, 73.2% and 65.6%, respectively. Among the remaining five parameters, the angle between the projection of the anchor chain in the horizontal plane and the direction of the wave β and the distance between two floats D also have moderate effects on the captured power, while the PTO stiffness K, the angle between the anchor chain and the plumb line α and the angle between the direction of wave propagation and that of the current γ have minor impacts on the captured power.

Comparing with the results of individual parameter influence on the captured power, the similarity is that the influence of wave height H is always the largest, and the buoy's radius R, the current velocity V, and PTO damping Call have great impacts on the captured power. However, when considering the influence of multi-parameter, the effects of the angle between the direction of wave propagation and that of the current γ is minor, and the influence of the angle between the projection of the anchor chain in the horizontal plane and the direction of the wave $\beta$are moderate, compared with major influence of γ and minor influence of β on the captured power in individual parameter impact analysis. These results indicate that the individual parameter influence on the captured power cannot only be considered during the WEC optimization, and the comprehensive influence of multi-parameter on the captured power of the WEC is not negligible.

4 | MODEL EXPERIMENT

To prove the effectiveness of the numerical analysis, a 1:20 scale model experiment was also conducted. As shown in Figure 8, the physical model consists of a cylindrical floater and a spheri-

TABLE 5 Effects of the parameter on the maximum captured power

Parameter	Level 1 (W)	Level 2 (W)	Level 3 (W)	Level 4 (W)	Range (W)	Effect (%)
R(m)	3186	3965	2514	1061	2904	73.2%
D(m)	3051	3112	2795	1768	1344	43.2%
C(N·s/m)	1067	2489	3990	3180	2923	73.3%
K(N/m)	2520	3027	2878	2301	726	24.0%
V(m/s)	4394	3259	1510	1563	2884	65.6%
H(m)	150	1711	3025	5840	5690	97.4%
α(°)	2218	3230	2193	3086	1037	32.1%
β(°)	2131	1917	2984	3695	1778	48.1%
γ(°)	2838	2424	3222	2232	990	30.7%

FIGURE 8 Setup of the model experiment

cal submerged body with the same radius 10 cm, fixed onto the floor of the wave-current tank by four tensioned anchor chains in a water depth of 1.5 m. There is a wave generator at one end of the tank, which can produce regular waves according to the needs of the test. The other end of the tank is equipped with porous wave absorption materials, in order to effectively reduce the reflection of the waves. The current generating system is also set at one end of the tank, and the adjustment of current velocity is realized by controlling the motor speed of the water pump. Because this experiment focused on the main parameters affecting the captured power, the wave height H and current velocity V were considered. In addition, the distance between two buoys D, a parameter of moderate influence, was also included for comparison. Note that the two buoys were connected by a spring, so the influences of the PTO damping C and the PTO stiffness K on the captured power were not considered in this experiment. The detailed parameter settings of H, V, D corresponding to the wave frequencies 0.9 and 1.2 Hz, respectively, are listed in Table 6. According to the Froude scaling law, the wave frequencies 0.9 and 1.2 Hz correspond to the wave frequencies 0.2 and 0.275 Hz in the target sea area, respectively.

TABLE 6 Parameter settings of the model experiment

Wave frequency (Hz)	H(cm)	V(m/s)	D(cm)
0.9, 1.2	0–6	0	15
0.9, 1.2	3	0–0.3	15
0.9, 1.2	3	0	5–20
0.9, 1.2	3	0	15

During the experiment, two high-speed cameras were used to capture the three-axis displacement of the two floats with sampling frequency 160 Hz, and then the relative velocity of the two floats was calculated. Since the PTO damping in this experiment was negligible, according to Equation (8), the captured power was represented by the square of the relative speed of the two floats.

Figure 9 shows the effects of three parameters on the square of the relative speed. For both wave frequencies, 0.9 and 1.2 Hz, as the wave height and current velocity increase, so does the captured power. By contrast, as the distance between the two buoys increases, the captured power first increases and then decreases. The most relevant parameter is the wave height, followed by the current velocity and the distance between the two buoys. Moreover, he captured power is greater at a wave frequency of 1.2 Hz than at 0.9 Hz. The results of the model experiment are consistent with those of the numerical simulation.

5 | PARAMETER OPTIMIZATION

According to the single and multi-parameter studies on the captured power of the WEC, the optimal combination of the principal parameters for the converter in real sea conditions in Zhaitang Island, China can be determined to maximize the output power. The following parameter design schemes are proposed:

- As the wave frequency of the target sea region mostly concentrates in 0.25–0.4 Hz, the optimal buoy's radius is set to 2–3 m to be able to capture the most power.

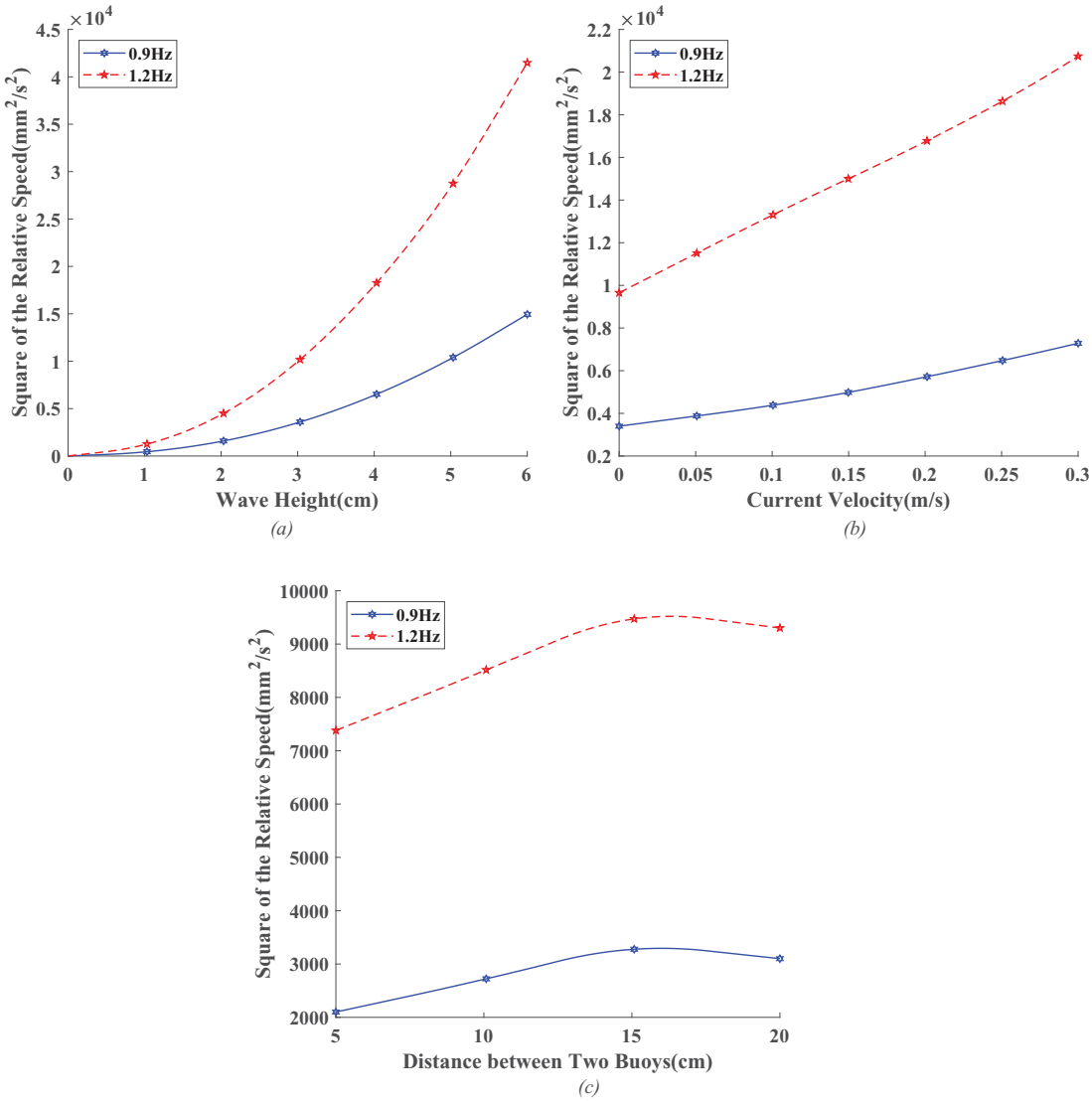

FIGURE 9 Parameter effects of the model experiment

- In the study of the influence of individual parameter, it is found that the device has its highest captured power when the PTO damping is in the range of 9000–15,000 N s/m, while in the multi-parameter study, the captured power is highest when the PTO damping is 15,000 N s/m, which is caused by the mutual influence of several parameters. Therefore, the PTO damping should be set to 15,000 N s/m.
- Although the angle between the projection of the anchor chain on the horizontal plane and the incident wave direction has no obvious effect on the captured power of the device in the study of the influence of individual parameters, in the comprehensive multi-parameter influence analysis it is found that this angle has a moderate impact on the captured power. Hence, this angle is recommended to be set to 45°.
- The wave height and current velocity have greater impacts on the captured power of the WEC and are positively correlated, especially when the directions of wave and current coincide. Considering the real sea conditions, the directions of wave and current of the sea area where the WEC is considered to be deployed may not be the same, so their angle should be set to be as small as possible. In addition, the wave height and current velocity should be as large as possible.

6 | CONCLUSIONS

The influences of individual parameters and multi-parameter on a two-body WEC in the target sea region of Zhaitang Island, China are presented. Nine parameters are considered: the buoy's radius R, the distance between two buoys D, the PTO damping C, the PTO stiffness K, the current velocity V, the wave height H, the angle between the anchor chain and the plumb line α, the angle between the incident wave direction and the projection of the anchor chain on the horizontal plane β, the angle between the incident wave direction and the current γ.

In order to predict the captured power more accurately with the variation of nine parameters as well as wave frequencies, the BP neural network is applied during the individual parameter influence analysis. The robust design method is used to analyse the comprehensive influences of nine parameters on the captured power. Furthermore, the model experiment in the wave-current tank is carried out to verify the effect of several main parameters on the captured power of the device. Numerical and experimental results indicate that, among the nine parameters, the H, C, R and V have the greatest influence on the captured power of the two-body WEC.

For the target sea region of Zhaitang Island, China, the schemes of optimal combination of parameters are proposed. The proposed parametric study approach can also provide references for two-body WEC designs in other sea regions. Note that the optimization analysis in this study is conducted based on normal sea conditions. The ranges considered for the environmental variables (wave height and period, current velocity) were selected to represent typical conditions in the area of interest. The optimization considering all the sea states over a long period of time (one year or longer) will be undertaken in future.

ACKNOWLEDGMENTS

This research was supported by the National Natural Science Foundation of China (Grant No. 51979283), the Shandong Provincial Natural Science Foundation, China (Grant No. ZR2018MEE053), the Fundamental Research Funds for the Central Universities (Grant No. 20CX02313A), and the Opening Fund of National Engineering Laboratory of Offshore Geophysical and Exploration Equipment (Grant No. 20CX02313A).

ORCID

Xingxian Bao https://orcid.org/0000-0002-8555-8366

REFERENCES

1. Xi, J.P.: Full text of Xi's statement at the General Debate of the 75th Session of the United Nations General Assembly. People's Daily Online Sept. 23 (2020)
2. Greaves, D., Iglesias, G.: Wave and Tidal Energy. John Wiley & Sons, Hoboken, NJ (2018)
3. Drew, B., et al.: A review of wave energy converter technology. Proc. Inst. Mech. Eng., Part A: J. Power Energy 223(8), 887–902 (2009)
4. Erselcan, I.O., Kükner, A.: A parametric optimization study towards the preliminary design of point absorber type wave energy converts suitable for the Turkish coasts of the Black Sea. Ocean Eng. 218, 108275 (2020)
5. Zhang, W.C., et al.: Hydrodynamic analysis and shape optimization for vertical axisymmetric wave energy converters. China Ocean Eng. 30(6), 954–966 (2016)
6. Wang, L., Yeung, R.W.: An efficient hybrid integral-equation method for point-absorber wave energy converters with a vertical axis of symmetry. Appl. Ocean Res. 86, 195–206 (2019)
7. Zheng, Y.H., et al.: Wave radiation by a floating rectangular structure in oblique seas. Ocean Eng. 33(1), 59–81 (2006)
8. Zheng, S., Zhang, Y.: Wave radiation from a truncated cylinder in front of a vertical wall. Ocean Eng. 111, 602–614 (2016)
9. Shen, Y.M., et al.: On the radiation and diffraction of linear water waves by a rectangular structure over a sill. Ocean Eng. 32(8-9), 1073–1097 (2005)
10. Zheng, S., Zhang, Y.: Wave diffraction from a truncated cylinder in front of a vertical wall. Ocean Eng. 104, 329–343 (2015)
11. Guo, B., Patton, R.J.: Non-linear viscous and friction effects on a heaving point absorber dynamics and latching control performance. IFAC-PapersOnLine 50(1), 15657–15662 (2017)
12. Guo, B., et al.: Nonlinear modeling and verification of a heaving point absorber for wave energy conversion. IEEE Trans. Sustainable Energy 9, 453–461 (2018)
13. Shadman, M., et al.: A geometrical optimization method applied to a heaving point absorber wave energy converter. Renewable Energy 115, 533–546 (2018)
14. Sergiienko, N.Y., et al.: An optimal arrangement of mooring lines for the three-tether submerged point-absorbing wave energy converter. Renewable Energy 93, 27–37 (2016)
15. Sergiienko, N.Y., et al.: Feasibility study of the three-tether axisymmetric wave energy converter. Ocean Eng. 150, 221–233 (2018)
16. Meng, F., et al.: Modal analysis of a submerged spherical point absorber with asymmetric mass distribution. Renewable Energy 130, 223–237 (2019)
17. Gao, H., Yu, Y.: The dynamics and power absorption of cone-cylinder wave energy converters with three degree of freedom in irregular waves. Energy 143, 833–845 (2008)
18. Goggins, J., Finnegan, W.: Shape optimisation of floating wave energy converters for a specified wave energy spectrum. Renewable Energy 71, 208–220 (2014)
19. Do, D.K.: Nonlinear control with wave observer to maximize harvested power for point absorber wave energy converters. Asian J. Control 47, 1–30 (2020)
20. Ringwood, J., et al.: An analytical and numerical sensitivity and robustness analysis of wave energy control systems. IEEE Trans. Control Syst. Technol. 99, 1–12 (2019)
21. Liang, C., Zuo, L.: On the dynamics and design of a two-body wave energy converter. Renewable Energy 101, 265–274 (2017)
22. Falnes, J.: Wave-energy conversion through relative motion between two single-mode oscillating bodies. J. Offshore Mech. Arct. Eng. 121, 32–38 (1999)
23. Beatty, S.J., et al.: Experimental and numerical comparisons of self-reacting point absorber wave energy converters in regular waves. Ocean Eng. 104, 370–386 (2015)
24. Candido, J.J., Justino, P.: Modelling, control and Pontryagin Maximum Principle for a two-body wave energy device. Renewable Energy 36(5), 1545–1557 (2011)
25. Shami, E.A., et al.: A parameter study and optimization of two body wave energy converters. Renewable Energy 131, 1–13 (2019)
26. Muliawan, M., et al.: Analysis of a two-body floating wave energy converter with particular focus on the effects of mooring systems on energy capture. J. Offshore Mech. Arct. 135(3), 317–328 (2013)
27. Martin, D., et al.: Numerical analysis and wave tank validation on the optimal design of a two-body wave energy converter. Renewable Energy 145, 632–641 (2019)
28. ANSYS,Inc.: Aqwa User's Manual. ANSYS, Inc., Canonsburg, PA (2021)
29. Cummins, W.E.: The impulse response function and ship motions. Schiffstechnik 9, 101–109 (1962)
30. Armesto, J.A., et al.: Comparative analysis of the methods to compute the radiation term in Cummins' equation. J. Ocean Eng. Mar. Energy 1, 377–393 (2015)
31. Wu, L., et al.: Parameter optimization for FPSO design using an improved FOA and IFOA-BP neural network. Ocean Eng. 175, 50–61 (2019)
32. Roy, R.K.: A Primer on the Taguchi Method. p. 247. Van Nostrand Rheinhold, New York (2010)

How to cite this article: Bao X., et al.: Parametric study and optimization of a two-body wave energy converter. IET Renew. Power Gener. 2021;15:3319–3330. https://doi.org/10.1049/rpg2.12254.